Post-collision interaction in Auger-electron emission of rare-gas atoms following electron-impact ionization

H. Ishii,* Y. Iketaki,† T. Watabe, T. Takayanagi, K. Wakiya, and H. Suzuki
Department of Physics, Sophia University, Chiyoda-ku, Tokyo 102 Japan

F. Koike
School of Medicine, Kitasato University, Sagamihara, Kanagawa 228 Japan
(Received 7 February 1990; revised manuscript received 10 September 1990)

A study of post-collision interaction has been carried out experimentally for Auger-electron emission of rare-gas atoms following electron-impact ionization. Spectra of the Xe $N_5O_{23}O_{23}$ ($^1S_0$), Kr $M_5N_1N_{23}$ ($^1P_1$), and Ar $L_3M_{23}M_{23}$ ($^1S_0$) Auger electrons have been measured changing the electron-impact energy from slightly above the threshold of the ionization to a few kilo-electron-volts. The Auger line shape has been analyzed using a profile formula that includes the finiteness of the velocities of all the cooperating electrons. Moreover, the analysis has partly considered the possible energy distribution of the scattered primary electron and the ejected secondary electron, due to the sharing of excess energy between them. The post-collision interaction effect is found to be absent at high excess energies.

I. INTRODUCTION

During the past two decades, the post-collision interaction (PCI) effect has been observed in various atomic processes, such as electron-impact autoionization,[1] Auger processes after photoionization,[2–6] Auger processes after electron-impact ionization,[7–16] and Coster-Kronig processes after electron-impact ionization.[17] Theoretical studies have also been made extensively.[18–25]

One of the main interests in recent years is the high-energy behavior of PCI. In 1983, Ogurtsov[26] formulated a classical model taking into account the time delay of the screening of the core charge by the ejected secondary electron (and the scattered primary electron if any). He pointed out that there was a constant negative displacement in the PCI shift from its $-\frac{1}{2}$ power law[27] of the excess energy. Russek and Melhhorn[28] proposed a formula which gave the PCI spectral profile including the time-delay effect. The validity of their semiclassical formalism, however, was questioned by Koike,[25] who proposed a wave-packet formalism for the PCI effect.

In the case of photoionization, the disappearance of the PCI effect at high excess energies was verified experimentally by Borst and Schmidt[29] and Armen *et al.*[30]

In the case of electron-impact ionization, however, the experiments have not yet converged. On the one hand, Iketaki *et al.*[16] observed that the Ar $L_3M_{23}M_{23}$ ($^1S_0$) Auger line became completely Lorentzian at the high excess energies they studied. On the other hand, Graef and Hink[15] reported that the PCI shift remained constant at high excess energies for the Ne $KL_{23}L_{23}$ ($^1D_2$) Auger line; Huster, Sandner, and Melhhorn[31] and Graef and Hink[32] also discussed this remaining constant PCI shift, assuming that the $-\frac{1}{2}$ power law holds. They clarified that a constant PCI shift must remain at high excess energies for their data to be consistent with their assumption. Theoretically, Sandner[33] pointed out that the ejected electron could always have a slow component created by the glancing primary electron, and that this slow component caused a finite PCI shift even at high excess energies. Sandner and Voelkel[34] have further pointed out that also the line shape does not converge to a Lorentzian. To evaluate the PCI effect, Sandner and his coworker,[33,34] have used the Russek and Mehlhorn formula,[28] which does not necessarily give the $-\frac{1}{2}$ power law for the PCI shift. Sandner and his coworker's argument is not directly comparable with the result of Hink and his coworkers. Further, the Sandner and Voelkel[34] prediction could be verified by neither Iketaki *et al.* experiment,[16] nor by the present experiment.

In the present paper, we describe the measurements of energies and profiles of the Xe, Kr, and Ar Auger lines produced by electron-impact ionization, and also present an elaborate profile analysis of the Xe $N_5O_{23}O_{23}$ ($^1S_0$), Kr $M_5N_1N_{23}$ ($^1P_1$), and Ar $L_3M_{23}M_{23}$ ($^1S_0$) Auger lines. The result of the Ar measurement has been partly reported[16] in one of the papers by our group; we refer to the paper as I from now on. In Sec. II we describe our experimental apparatus and procedure. In Sec. III we give our experimental results. In Sec. IV we present our Auger spectral profiles and their analysis. We summarize our understanding for the PCI effect in Sec. V.

II. EXPERIMENTAL APPARATUS AND PROCEDURE

To perform our experiment, two slightly different types of apparatus were used; one for Xe and Kr, and the other for Ar.

A. Experimental setup for Xe and Kr

We employ a crossed-beam-type apparatus. A primary electron beam is produced by a thermoelectronic-

emission-type electron gun, which is tuned to supply an adequate stable current at each acceleration voltage. We obtain an electron current ranging from 11.5 to 82 μA for the Xe measurement, and from 27 to 300 μA for the Kr measurement. The energy resolution of the analyzer is independent of the electron current, but the current is carefully kept constant throughout the experiment to avoid any unexpected instability of the apparatus. The electron beam perpendicularly crosses the target-gas beam.

Electrons ejected with an angle 120° with respect to the direction of the primary electron beam are decelerated to 1.5 eV and led into the energy analyzer. Potentials on the lens system, which consists of four cylindrical electrodes, are scanned with the decelerating voltage, so that the transmission efficiency through the lens is kept constant over a wide energy range, as far as possible. We use a hemispherical electrostatic analyzer with a mean radius of 50 mm. The energy resolution is about 65 meV in the Xe measurement and about 60 meV in the Kr measurement in full width at half maximum (FWHM). The precise values of the energy resolution are so evaluated at high impact energies that the width of the convoluted Lorentzian of natural linewidth with the instrumental Gaussian line profile gives the best fit to the apparent experimental Auger linewidth. The electrons after the analyzer are detected by a channel electron multiplier. The Earth's magnetic field is canceled by a Helmholtz coil and screened by a μ-metal shield.

To compensate for the unavoidable drifting of the experimental conditions, we performed data acquisition in the following way. First, the electron energy scanning time was short, e.g., 10 ms/channel, and several hundred scans were stored as one set. Second, to improve statistics, several sets of scans were summed, and, in the course of the summation, the measured electron energy was so corrected as to give a maximum overlap with the preceding partial sum.

To calibrate the Auger-electron energy, we used the autoionization line He $2s2p(^1P)$ at 35.54 eV as a standard, which is the difference of the excitation energy of 60.123 eV (Ref. 35) and the He ionization potential of 24.580 eV.[36] Because the lowest impact energy of the electrons in the present experiment was as high as 77.8 eV, the energy position of this standard line was free from the PCI effect.[1] As the target-gas beam, we used the gas mixture composed of Xe and He or Kr and He. The gas mixing ratio was carefully kept constant during a series of measurements. For the spectral profile analysis, we also measured the spectra without the He gas for the Kr Auger transition, because there was an overlap of the He autoionization lines with the Kr Auger lines.

To calibrate the impact electron energy, we compared the energy of the elastically scattered primary electrons with the peak positions of the He autoionizing electrons on the same spectrum. The calibration was made for primary electrons whose excess energies above the thresholds were lower than 30 eV, and the differences between the electron-beam energies and the acceleration voltages were about 1 eV.

B. Experimental setup for Ar

Because our apparatus for the Ar measurement is similar to that for the Xe and Kr measurement, we describe here only the differences. Here we use a 127° coaxial cylindrical electrostatic analyzer with the mean radius of 50 mm. Its energy resolution is 140 meV in FWHM, which was determined by observing the apparent width of a shake-off Ar Auger line $L_{23}M_{23}(^3D_3)$-$M_{23}M_{23}M_{23}(^2P)$ at 190.70 eV. The natural width of this line is theoretically predicted to be as narrow as 9.4 meV.[37] As the reference lines for the calibration of Auger-electron energy, we used both the Ar $3s3p^64p(^1P)\rightarrow 3s^23p^5(^2P_{3/2})$ autoionization line at 10.86 eV, and the He $2s2p(^1P)\rightarrow 1s(^2S)$ autoionization line at 35.54 eV.

III. EXPERIMENTAL RESULT

In Figs. 1–3, we show typical examples of the Auger-electron spectrum. Figure 1 gives the Xe $N_{4,5}OO$

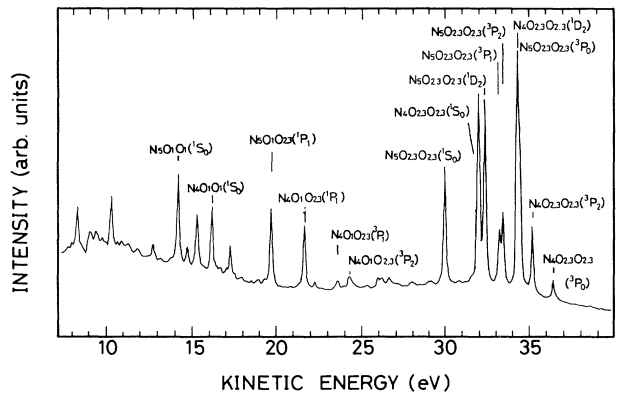

FIG. 1. Panorama of the Xe $N_{4,5}$ OO Auger-electron spectra. The primary electron-impact energy is 2 keV. The observation angle is 120° with respect to the primary electron beam direction.

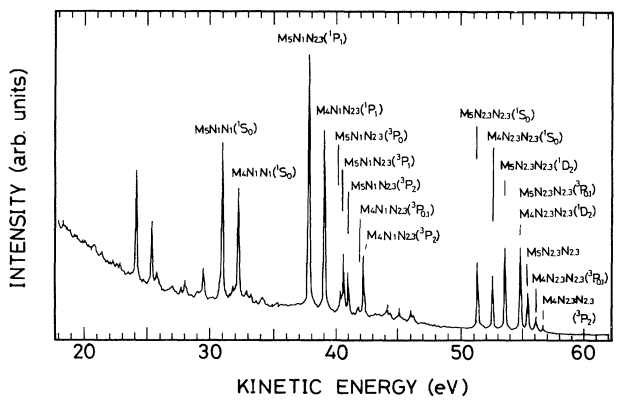

FIG. 2. Panorama of the Kr, $M_{4,5}NN$ Auger-electron spectra. The primary electron-impact energy is 2 keV. The observation angle is 120° with respect to the primary electron beam direction.

Auger-electron spectrum produced by the impact of the electrons with the energy of 2 keV. Figure 2 gives the Kr $M_{4,5}NN$ Auger-electron spectrum produced by the impact energy of 2 keV, and Fig. 3 gives the Ar $L_{2,3}MM$ Auger-electron spectrum produced by the impact energy of 5 keV. A number of Auger lines are identified, and their energy positions are determined from the spectra obtained at the highest electron-impact energies, which were 4.93 keV for Xe, 5.9 keV for Kr, and 1.75 keV for Ar, respectively. Table I summarizes our measurement of the energy positions of the Auger transitions, together with the data of other authors. The accuracy of the energy values is estimated to be ±0.02 eV for Xe *NOO* and Kr *MNN* Auger lines, and ±0.05 eV for Ar *LMM* Auger lines, respectively. As will be discussed later, we found no evidence for the constant PCI shift of the spectral peak positions at the highest electron-impact energies. The values listed in Table I are interpreted as the nominal peak energies. The values for Xe *NOO* and Kr *MNN* Auger lines are in overall agreement with those determined by Ohtani *et al.*,[7] which are larger than the values of Siegbahn *et al.*[38] by 0.20±0.03 eV systematically, as pointed out by Ohtani *et al.*[7]

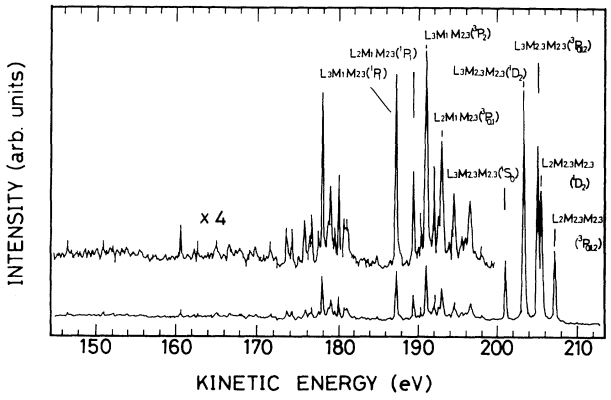

FIG. 3. Panorama of the Ar $L_{2,3}MM$ Auger-electron spectra. The primary electron-impact energy is 5 keV. The observation angle is 120° with respect to the primary electron beam direction.

We have further investigated the spectral peak profiles and their energy positions for selected Auger lines in detail by changing the primary electron-impact energy. The impact energy dependence of the Xe $N_5O_{23}O_{23}$ ($^1S_0$) Auger line shape is illustrated in Fig. 4. The relative intensity of the Auger electrons are plotted as functions of kinetic energies for various excess energies, which mean the impact energies subtracted by the 4*d* ionization energy in Xe, ranging from 10.2 eV up to 4.93 keV. The vertical line at 29.97 eV indicates the nominal kinetic energy of the Auger electron. The solid lines and the broken lines are theoretical, which will be discussed in detail in Sec. IV. We see in Fig. 4 that the spectral profile becomes almost symmetric with respect to the peak center when the excess energy exceeds twice the nominal kinetic energy of Auger electrons. This strongly suggests the disappearance of the PCI effect in the high-excess-energy region. The impact energy dependence of the Kr $M_5N_1N_{23}$ ($^1P_1$) Auger line shape is plotted in Fig. 5, where the nominal energy of the Auger line is 37.84 eV. We see also in the Kr case that the line shape is completely symmetric with respect to the peak center in the high-excess-energy region. But at the same time, we find that a slight asymmetry remains at an energy region

TABLE I. Nominal energy positions of the Auger electrons in units of eV. Figures in the parentheses are errors; e.g., 29.73(4) should read as 29.73±0.04.

Auger line	Present	ESCA[a]	Author Ohtani[b]	Mehlhorn[c]	Johansson[d]
Xe $N_5O_{23}O_{23}$ ($^1S_0$)	29.97(2)	29.73(4)	29.91(3)		
Xe $N_4O_{23}O_{23}$ ($^1S_0$)	31.95(2)	31.71(4)	31.90(3)		
Xe $N_5O_{23}O_{23}$ ($^1D_2$)	32.33(2)	32.09(3)	32.38(3)		
Xe $N_5O_{23}O_{23}$ ($^1S_0$)	33.44(2)	33.21(5)	33.42(3)		
Xe $N_5O_{23}O_{23}$ ($^1S_0$)	34.31(2)	34.07(5)	34.28(3)		
Xe $N_5O_{23}O_{23}$ ($^1S_0$)	34.45(2)	34.21(5)	34.40(3)		
Kr $M_5N_1N_{23}$ ($^1P_1$)	37.84(2)	37.67(10)	37.87(3)	37.67	
Kr $M_4N_1N_{23}$ ($^1P_1$)	39.09(2)	38.91(10)	39.08(3)	38.91	
Ar $L_3M_{23}M_{23}$ ($^1S_0$)	201.08(5)	201.09(20)			201.10(10)
Ar $L_3M_{23}M_{23}$ ($^1D_2$)	203.45(5)	203.47(20)			203.49(10)
Ar $L_3M_{23}M_{23}$ (^3P)	205.18(5)	205.21(20)			205.22(10)
Ar $L_2M_{23}M_{23}$ ($^1D_2$)	205.59(5)	205.62(20)			205.61(10)
Ar $L_2M_{23}M_{23}$ (^3P)	207.19(5)	207.23(20)			207.25(10)

[a]Reference 38.
[b]Reference 7.
[c]Reference 39.
[d]Reference 40.

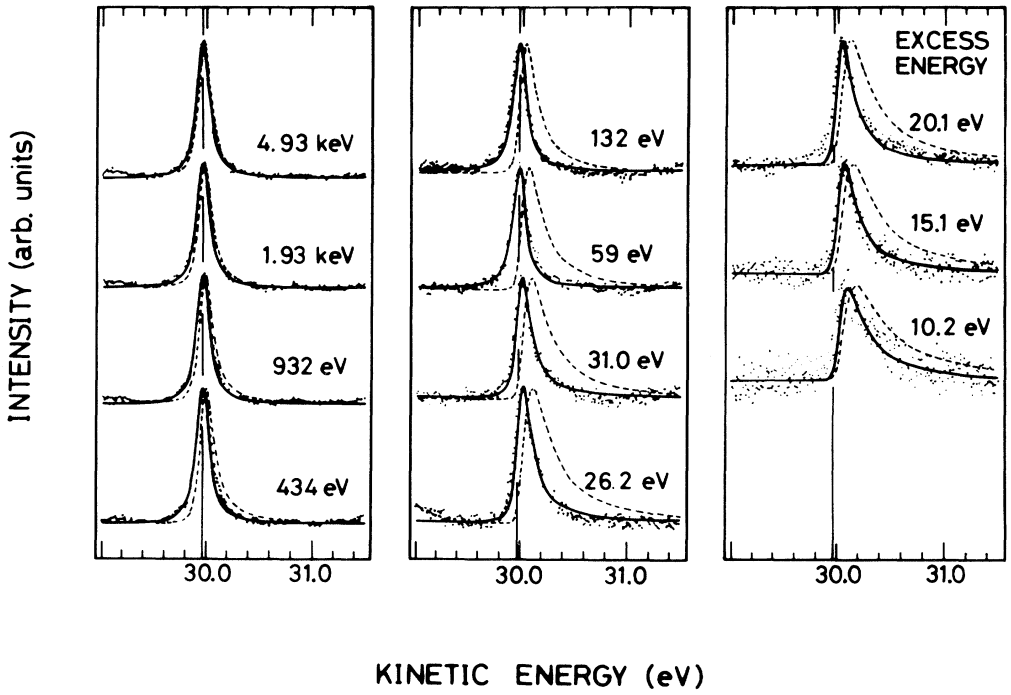

FIG. 4. The primary electron-impact energy dependence of the Xe $N_5O_{23}O_{23}$ ($^1S_0$) Auger line shape. Dots are the experimental line shape. The energy value indicated at each line represents the excess energy, i.e., the difference of the primary electron-impact energy from the ionization threshold energy. The vertical line near the spectral peak indicates the nominal position of the Auger transition energy. The solid lines are of the empirical formula of I, i.e., of Eq. (1) with Eq. (4). The dashed lines are of the semiclassical model.

above twice the nominal kinetic energy of the Auger electrons, e.g., at the excess energies from 100 to 200 eV. We will discuss this point in detail in Sec. IV. Figure 6 shows the impact energy dependence of the Ar, $L_3M_{23}M_{23}$ ($^1S_0$) Auger line shape by dots, where the nominal energy of the Auger line is 201.08 eV. Again, we find the disappearance of the asymmetry of the spectral peak shape at excess energies higher than twice the nominal kinetic en-

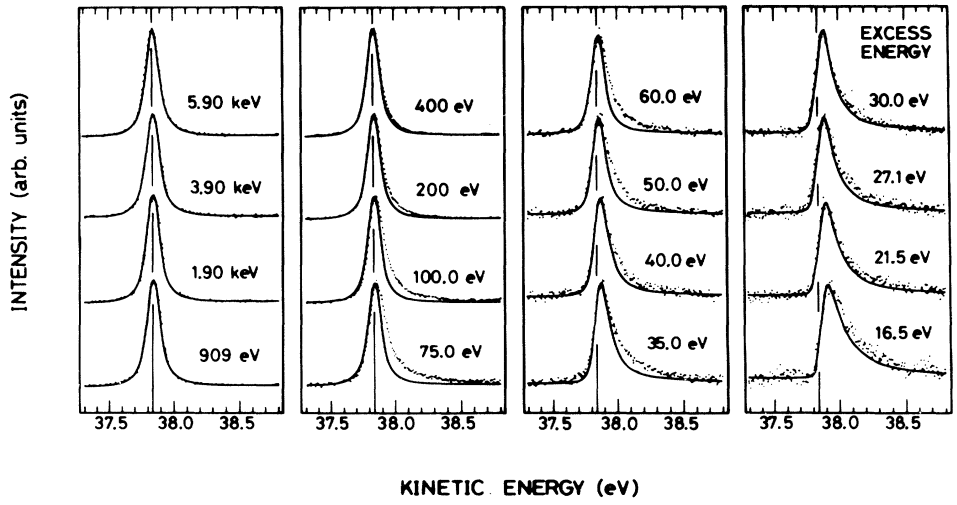

FIG. 5. The primary electron-impact energy dependence of the Kr $M_5N_1N_{23}$ ($^1P_1$) Auger line shape. For notations, see Fig. 4.

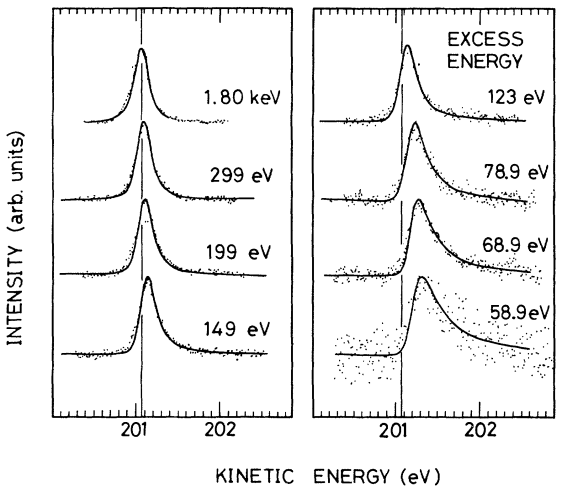

FIG. 6. The primary electron-impact energy dependence of the Ar $L_3M_{23}M_{23}$ ($^1S_0$) Auger line shape. For notations, see Fig. 4.

ergy of the Auger electrons. Figure 6 is essentially the same as Fig. 2 in I.

IV. SPECTRAL PROFILE ANALYSIS

As for the isolated Auger lines under the influence of the scattered and ejected electrons, we have proposed an empirical profile function, Eqs. (1) and (2) in I, which represents an intensity of the Auger electrons against the kinetic energy of the Auger electrons. This profile function is a modification of the semiclassical profile function[20,21] by taking into account the time delay for the Auger electron to overtake the scattered and ejected electrons. One of the present authors (Koike[25]) has recently derived a profile function quantum mechanically; we refer to this paper as II from now on. The profile function is given by [atomic units ($e=m=\hbar$) are used throughout this paper, unless otherwise stated]

$$P(E_A;Q)=\frac{\pi Q\exp(\pi Q)}{\sinh(\pi Q)}\frac{\exp(-2Q\arg z)}{|z|^2}\ , \tag{1}$$

with

$$z=(E_A-E_0)+i\Gamma/2\ , \tag{2}$$

and

$$Q=\max\left[0,\frac{v_A-v_{ra}}{v_A v_{ra}}\right]+\max\left[0,\frac{v_A-v_{rb}}{v_A v_{rb}}\right]\ , \tag{3}$$

where $P(E_A;Q)$ is the profile function, i is the imaginary unit, z is a complex energy, which consists of Auger-electron energy E_A, nominal Auger-electron energy E_0, and the natural energy width of the Auger transition Γ, Q is a parameter which is given by a function of the Auger-electron nominal velocity v_A and the velocities of the scattered and ejected electrons v_{ra} and v_{rb}, respectively, and max indicates the larger of the arguments. In II, it has been pointed out that the empirical formula in I may be obtained by putting $v_{ra}=v_{rb}\equiv v_r$; the empirical formula corresponds to a Wannier[41] case assumption to Eq. (1). In this case we have

$$Q=2\max\left[0,\frac{v_A-v_r}{v_A v_r}\right]\ . \tag{4}$$

The semiclassical model may be derived by assuming that $v_A\gg v_r$ in Eq. (4), i.e., by taking $Q=2/v_r$.

In actual Auger-electron emission caused by electron-impact ionization, the parameter Q may take various values due to the sharing of the energy between the scattered and the ejected electrons; the profile function $P(E_A;Q)$ in Eq. (1) is the formula for one single-collision event with a specific energy partitioning between the two electrons. We take E_{ex} as the excess energy, i.e., the difference of the impact energy of the primary electron from the threshold energy of the inner-shell ionization. The parameter Q may take a value that satisfies the following constraint; that is,

$$E_{ex}=\tfrac{1}{2}v_{ra}^2+\tfrac{1}{2}v_{rb}^2\ . \tag{5}$$

If we take $d\sigma_Q/dQ$ as the differential inner-shell ionization cross section with respect to Q, we have

$$P_t(E_A)=\int P(E_A;Q)d\sigma_Q \tag{6}$$

for the total Auger line profile function $P_t(E_A)$, which may be observed by an Auger-electron counting without coincidence with the scattered or ejected electrons.

To compare the present experimental results with the theory, we first calculate Eq. (1) using Eq. (4); we calculate the profiles according to the Wannier case model. The results are shown in Figs. 4–6 as solid curves. For comparison, we also make a semiclassical calculation for Xe, which is shown in Fig. 4 as the dashed curves. The atomic parameters used in the present calculation are summarized in Table II. The natural PCI profile has been convoluted by a Gaussian-type experimental apparatus function. Optimum values for the FWHM of the apparatus function have been obtained by fitting the convoluted spectral peak profile to the experimental data, as was mentioned previously. The absolute magnitude of the spectral profile has been so normalized to the data, on the one hand, to have the same maximum intensity and, on the other hand, to gain a best fit at the ends of both spectral tails. To obtain the best fit, we have added a constant background intensity on each theoretical spectral profile; i.e., we have assumed that the background electron intensity can be regarded as constant in the energy range including a single Auger spectral peak. This assumption may be evaluated by investigating the overall features of the spectrum, of which three drawings are shown in Figs. 1–3. We have concluded that the assumption was adequate to the present case.

Comparing the solid and dashed lines in Fig. 4, we find that the semiclassical model is unsuccessful to reproduce the data. In fact, it gives us the idea that the simple $-\frac{1}{2}$ power law for the PCI shift does not work in the present case. On the other hand, we find in Figs. 4–6 that the

TABLE II. Constants for calculation: asterisk denotes taken from Ref. 43; dagger denotes calculated from E_0 using Ref. 36.

Species	Constants: Nominal Auger energy E_0 (eV)	Level width Γ (meV)	Threshold (eV)
Xe	29.97	129(8)*	67.548(11)*
Kr	37.84	98(12)*	93.788(20)*
Ar	201.08	135(8)*	248.56†

present model reproduces the experimental results quite well, except for the intermediate-excess-energy regions, namely, except for the values of E_{ex} from 59 to 434 eV in Xe, from 35 to 400 eV for Kr, and around 400 eV for Ar. The disagreement of the theory and the experiment in the intermediate energy region may be explained by considering the possible energy distribution of the scattered and the ejected electrons. We investigate this at the end of this section.

We have further obtained the PCI shifts of the spectral peak position as functions of the excess energies. Figure 7 shows the energy position of the Xe $N_5O_{23}O_{23}$ ($^1S_0$) Auger line. Figure 8 shows the energy position of the Kr $M_5N_1N_{23}$ ($^1P_1$) Auger line. Figure 9 shows the energy position of the Ar $L_3M_{23}M_{23}$ ($^1D_2$) Auger line. To evaluate the PCI shift, we have assumed that the PCI shift disappears at the highest-excess-energy region. In all the highest excess energies studied, we have obtained a perfect agreement of the experimental Auger spectral peak to a Lorentzian profile with the convolution of the Gaussian-type apparatus function; the spectral profile is completely symmetric with respect to the peak energy position.[42] As Sandner and Voelkel have shown recently,[34] the Auger line profile remains asymmetric if the PCI effect remains at the highest-impact-energy region. It is therefore reasonable to conclude that the spectral peak indicates the nominal energy position of the Auger transition at the highest impact energies in the present experiment. In Figs. 7–9, we have also plotted the theoretical PCI shifts; solid curves are of the empirical formula of I, namely, Eq. (1) with Eq. (4), and the dashed curves are of the semiclassical formula. The solid lines, indicated as $f1$, $f2$, and $f3$ in Fig. 8, are also theoretical, but we discuss them later. The empirical formula agrees fairly well with the present experimental results except for the intermediate electron-impact energies for Kr.

As the second step of the profile analysis, we have tried to consider the energy distribution of the scattered and ejected electrons. We have adopted the Kr spectrum to investigate this effect, because the deviation of the experimental profile from the empirical formula of I has been the most prominent in the Kr case. We have employed Eq. (6) to obtain a theoretical line profile. As the test, we choose three types of functions for the energy distribution $d\sigma_Q/dQ$. The first is a function with a maximum at half of the excess energy; $d\sigma_Q/dE = (d\sigma_Q/dQ)(dQ/dE) \propto 1-\cos(2\pi E/E_{ex})$, where E ($=\frac{1}{2}v_{ra}^2$ or $\frac{1}{2}v_{rb}^2$) is the kinetic energy of one of the receding electrons; we shall call this function (1) from now on. The function (1) simulates the situation where each receding electron has about half of the excess energy. The two receding electron tend to share the excess energy equally at low excess energies, obeying the Wannier threshold law. The second is a function that gives a

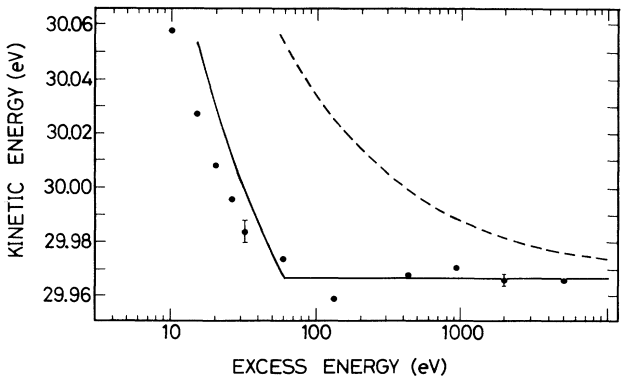

FIG. 7. The excess-energy dependence of the spectral peak position of the Xe $N_5O_{23}O_{23}$ ($^1S_0$) Auger line: closed circles, present experiment; solid line, empirical formula of I [Eq. (1) with Eq. (4)]; dashed line, semiclassical model.

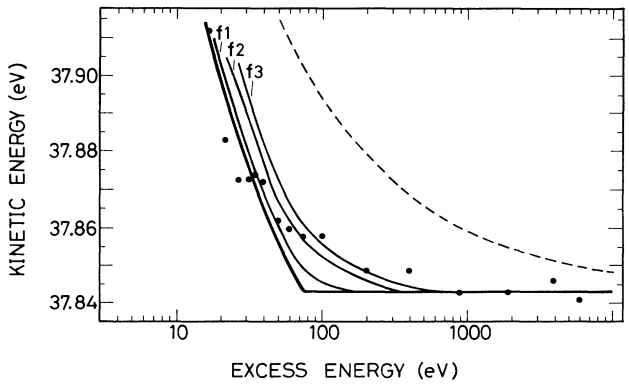

FIG. 8. The excess-energy dependence of the energy position of the Kr $M_5N_1N_{23}$ ($^1P_1$) Auger line: solid lines indicated as $f1$, $f2$, and $f3$ are of Eq. (6) with three kinds of model electron-energy distributions. For details, see text. For other notations, see Fig. 7.

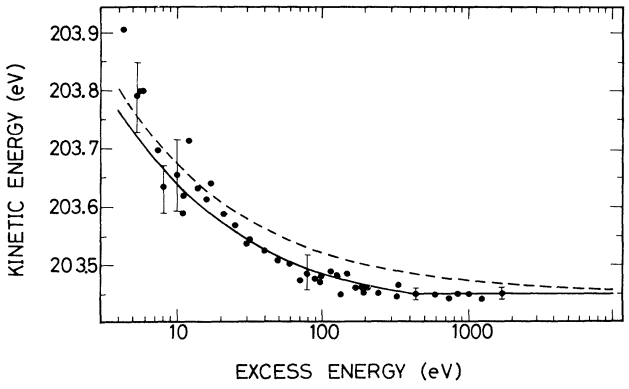

FIG. 9. The excess-energy dependence of the energy position of the Ar $L_3M_{23}M_{23}$ ($^1D_2$) Auger line. For notations, see Fig. 7.

uniform energy distribution of the receding electrons; we shall call this function(2) from now on. Function (2) is in the middle between the first and the third which is introduced in the followings. The third is a function of the Mott-type cross section;

$$\frac{d\sigma_Q}{dE} \propto \frac{1}{(E-B)^2} + \frac{1}{(E_{ex}+B-E)^2} + \frac{1}{(E-B)(E_{ex}+B-E)} , \tag{7}$$

where B is the binding energy of the inner-shell orbital; we shall call this function (3) from now on. At high excess energies, the Mott cross section gives a reasonable energy distribution of the secondary electrons over the whole range of the electron energy.[44] As a matter of fact, the Mott cross section depends on the primary electron-

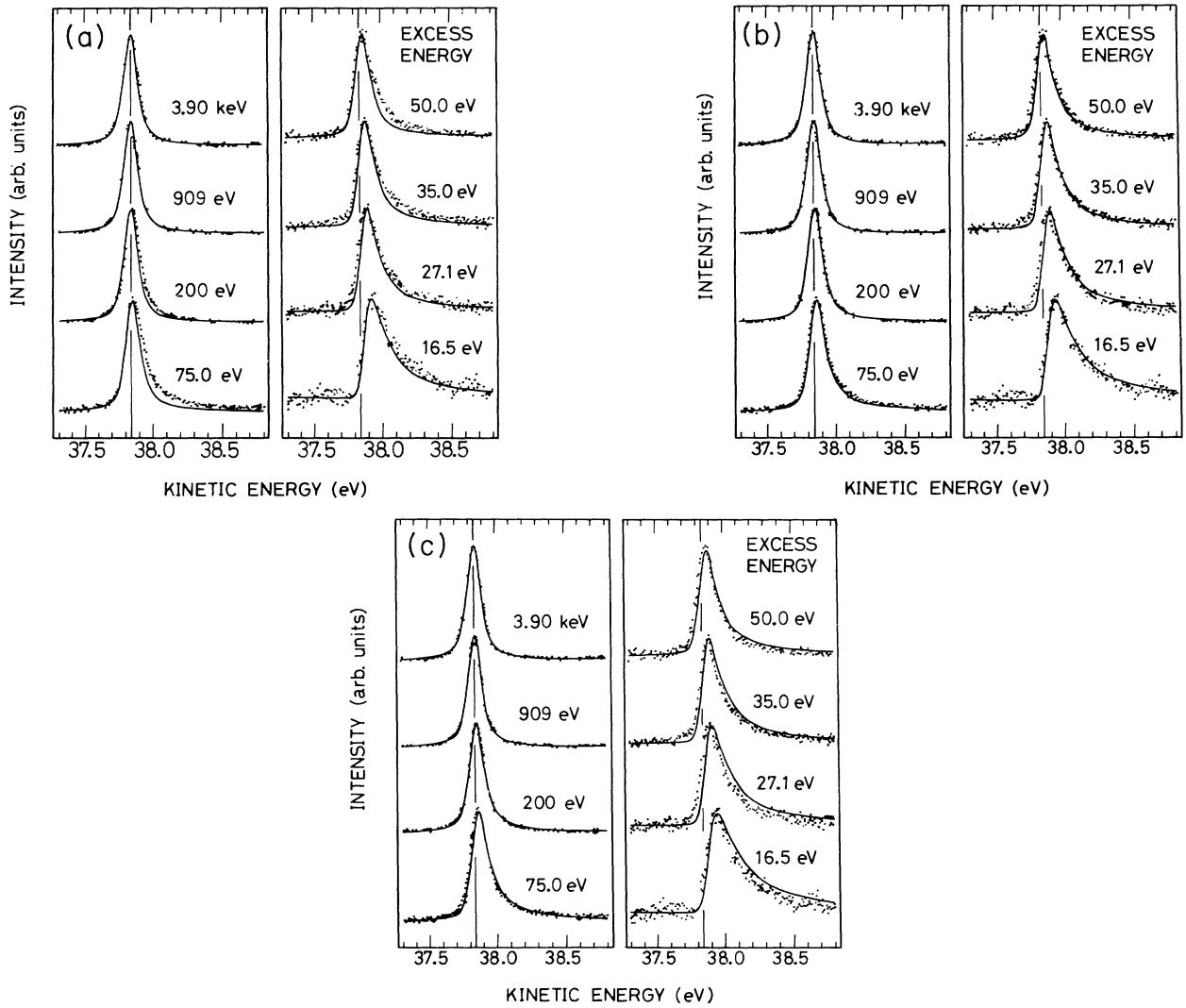

FIG. 10. The dependence of the Kr $M_5N_1N_{23}$ ($^1P_1$) Auger line shape on the energy distribution of the receding electrons: Dots are of the experiment; (a) theory with the distribution function (1); (b) theory with the distribution function(2); (c) theory with the distribution function (3).

impact energy $E_{ex}+B$. But for simplicity we apply the formula at a fixed primary electron-impact energy of 293.73 eV, of which corresponding excess energy E_{ex} is 200 eV. The actual energy distribution at desired impact energy point is obtained by scaling Eq. (7) in terms of E/E_{ex}. The result of the profile calculation using Eq. (6) is shown in Figs. 10(a)–10(c), together with the experimental profiles given by dots. Figure 10(a) stands for function (1), Fig. 10(b) stands for function (2), and Fig. 10(c) stands for function (3). We see clearly that function (1) gives excellent agreement of the Auger line profiles with the experimental results in the low-excess-energy region, and at the same time we see that function (3) also gives excellent agreement in the high-excess-energy region. Further, we see that the disagreement between the theory and experiment appeared in the intermediate-excess-energy region (see Fig. 5) has been much improved by an employment of function (2). We have also plotted the calculated PCI shift in Fig. 8. The solid lines indicated by $f1$, $f2$, and $f3$ represent the PCI shift obtained by the use of functions (1)–(3), respectively. We see that the line $f2$ reproduces well the experimental PCI shift in the intermediate-excess-energy region.

V. DISCUSSION

We have quantitatively studied the variation of the shift and the shape of the three typical Auger lines chosen from the Xe *NOO*, Kr *MNN*, and Ar *LMM* Auger transitions. The experimental spectral profiles have been compared with the theoretical profiles in two ways. First, we have used an empirical formula which has been proposed in I. Second, we have used Eq. (6) by taking into account the possible energy distribution of the receding electrons.

Concerning the high-excess-energy behavior of the Auger line profiles, we have found that they become Lorentzian with no exception in the three cases we have investigated. The real experimental line profile is modified by the apparatus function. To remove this, we had to optimize the unknown parameters in the apparatus function in the course of the profile fitting. Therefore there may be, in principle, a possibility that an asymmetry of the natural line profile is canceled out accidentally by the asymmetry of the apparatus function, but it is hard to suppose that such an accident could have taken place for all three Auger lines. We conclude that the PCI effect is practically absent in the high-excess-energy region. The present experimental results, therefore, do not appear to support the theoretical prediction by Sandner and Voelkel,[34] who have discussed the remaining PCI effect at the high-excess-energy limit. Our profile calculation for Kr by the use of three kinds of the energy distribution of the receding electrons has been also unsuccessful in reproducing an asymmetric line profile, even at the highest excess energies. The PCI effect could always remain, in general, at the high-excess-energy limit in the case of the electron-impact ionization, since the slow receding electron, which causes the PCI effect, could always be produced in the impact ionization process, but the effect seems to be so weak that it is unobservable within the accuracy of the present experiment.

Although it is not easy to resolve the origin of the discrepancy between the theory[34] and the present experiment, we can point out the following possibility, i.e., the effect of angular correlation between the secondary and the Auger electrons. Recently, van der Straten, Morgenstern, and Niehaus[45] studied the angular-dependent post-collision interaction, and they pointed out that the PCI shift of the peak position could be negative at smaller relative ejection angles between the Auger and the secondary electrons. Generally speaking, the high-energy primary electron is likely to eject the secondary electron in the direction of its momentum transfer, and hence the secondary electrons created by soft collisions are mainly ejected perpendicular to the primary beam direction. Since we observe the Auger electron at 120° with respect to the primary electron beam, the relative angles between the secondary and Auger electrons are typically 30° when both the electrons are ejected into the same side of the primary electron beam, and 150° when the two electrons are ejected into the opposite side of the primary electron beam. It might happen that the positive PCI shift is canceled out by the negative one, to place the Auger line at a neutral position. Because Sandner and Voelkel[34] assumed the isotropy of the secondary electron distribution, they could not consider this cancellation. It is meaningful to see what occurs when the isotropy assumption is removed to their calculation.

If there is no remaining PCI effect at the high-excess-energy region, there should also be no remaining PCI shift. In this sense, the result of the present profile analysis does not support the PCI-shift analysis by Graef and Hink.[15,32] They have performed the analysis based on their assumption that the PCI shift should be proportional to the $-\frac{1}{2}$ power of the excess energy. However, as Ogurtsov has predicted,[26] and as we also may conclude from Eq. (1), we certainly have a deviation from the $-\frac{1}{2}$ power law, if we take into account the delay for the Auger electron to overtake the receding electron. Generally speaking, it is not appropriate to extensively apply a formula based on a simple approximation that works only in a limited range of the variables. The $-\frac{1}{2}$ power law should have been questioned before the idea of the remaining constant PCI shift had been recognized. It seems to be necessary for their experimental data, which appear very precise, to be examined without assuming the $-\frac{1}{2}$ power law.

A most crucial point is the energy distribution of the receding electrons for the determination of whether the PCI effect remains at the high-excess-energy limit. We could, in principle, extract a plausible distribution from the spherical profile analysis, but we hesitate to carry it out, since there have been several assumptions and parameters chosen rather arbitrarily, for example, the instrumental response function, parameters used to synthesize the calculated line profile, and so on. We cannot expect that the addition of a more complicated assumption will bring us more fruitful results. It may be rather desirable to ascertain our profile formulas more generally for the cases of the Auger processes originating from vacancy states in deeper shells or Coster-Kronig transitions.

These works are planned to be issued by our group in a planned forthcoming paper.

ACKNOWLEDGMENTS

The authors are grateful to Professor S. Ohtani for his stimulating discussion. H.I. and T.W. wish to thank all the members of their laboratory for helpful suggestions and communications. In particular, they wish to give special thanks to Y. Tanaka for helping them with both the experiment and the data analysis. The authors are obliged to Professor A Fujii of Sophia University for his reading of the manuscript.

---

*Present address: Canon, Inc., Nakahara-ku, Kawasaki, Kanagawa 211, Japan.

†Present address: Olympus Optical Co., Ltd., Hachioji, Tokyo 192, Japan.

[1]J. Hicks, S. Cvejanovic, J. Comer, F. H. Read, and J. M. Sharp, Vacuum **24**, 573 (1974).

[2]M. J. van der Wiel, G. W. Wight, and R. R. Tol, J. Phys. B **9**, L5 (1976).

[3]G. W. Wight and M. J. van der Wiel, J. Phys. B **10**, 601 (1977).

[4]V. Schmidt, N. Sandner, W. Mehlhorn, M. Y. Adam, and F. Wuilleumier, Phys. Rev. Lett. **38**, 63 (1977).

[5]V. Schmidt, S. Krummacher, F. Wuilleumier, and P. Dhez, Phys. Rev. A **24**, 1803 (1981).

[6]H. Hanashiro, Y. Suzuki, T. Sasaki, A. Mikuni, T. Takayanagi, K. Wakiya, H. Suzuki, A. Danjo, T. Hoshino, and S. Ohtani, J. Phys. B **12**, L775 (1979).

[7]S. Ohtani, H. Nishimura, H. Suzuki, and K. Wakiya, Phys. Rev. Lett. **36**, 863 (1976).

[8]W. Hink, H. P. Schmidt, and T. Ebding, J. Phys. B **12**, L257 (1979).

[9]K. Wakiya, H. Suzuki, T. Takayanagi, M. Muto, S. Ito and Y. Iketaki, in *Proceedings of the Twelfth International Conference on the Physics of Electronic and Atomic Collisions, Abstracts of Contributed Papers, Gatlinburg, 1981,* edited by S. Datz (North-Holland, Amsterdam, 1981), p. 247.

[10]K. Helenelund, K. L. Tan, and U. Gelius, J. Phys. B **19**, 2659 (1986).

[11]S. Hedman, K. Helenelund, L. Asplund, U. Gelius, and K. Siegbahn, J. Phys. B **15**, L799 (1982).

[12]K. Helenelund, S. Hedman, L. Asplund, U. Gelius, and K. Siegbahn, Phys. Scr. **27**, 245 (1983).

[13]R. Huster and W. Mehlhorn, Z. Phys. A **307**, 67 (1982).

[42]D. Graef, thesis, Wuertsburg, 1986.

[15]D. Graef and W. Hink, J. Phys. B **19**, L221 (1986).

[16]Y. Iketaki, T. Takayanagi, K. Wakiya, H. Suzuki, and F. Koike, J. Phys. Soc. Jpn. **57**, 391 (1988).

[17]A. Yagishita, H. Hanashiro, S. Ohtani, and H. Suzuki, J. Phys. B **14**, L777 (1981).

[18]F. H. Read, Radiat. Res. **64**, 23 (1975).

[19]F. H. Read, J. Phys. B **10**, L207 (1977).

[20]A. Niehaus, J. Phys. B **10**, 1845 (1977).

[21]R. Morgenstern, A Niehaus, and U. Thielman, J. Phys. B **10**, 1039 (1977).

[22]T. Watanabe, T. Ishihara and J. Mizuno, J. Phys. B **16**, L107 (1983).

[23]P. Froelich, O. Goscinski, U. Gelius, and K. Helenelund, J. Phys. B **19**, 387 (1986).

[24]J. Tulkki, G. B. Armen, T. Aberg, B. Crasemann and M. H. Chen, Z. Phys. D **5**, 241 (1987).

[25]F. Koike, J. Phys. Soc. Jpn. **57**, 2705 (1988).

[26]G. N. Ogurtsov, J. Phys. B **16**, L745 (1983).

[27]R. B. Barker and H. W. Berry, Phys. Rev. **151**, 14 (1966).

[28]A. Russek and W. Mehlhorn, J. Phys. B **19**, 911 (1986).

[29]M. Borst and V. Schmidt, Phys. Rev. A **33**, 4456 (1986).

[30]G. B. Armen, S. L. Sorensen, S. B. Whitfield, G. E. Ice, J. C. Levin, G. S. Brown, and B. Crasemann, Phys. Rev. A **35**, 3966 (1987).

[31]R. Huster, W. Sandner, and W. Mehlhorn, J. Phys. B **20**, L287 (1987).

[32]D. Graef and W. Hink, J. Phys. B **20**, 2677 (1987).

[33]W. Sandner, J. Phys. B **19**, L863 (1986).

[34]W. Sandner and M. Voelkel, Phys. Rev. Lett. **62**, 885 (1989).

[35]R. P. Madden and K. Codling, Astrophys. J. **141**, 364 (1965).

[36]C. E. Moore, Atomic Energy Levels, (Natl. Bur. Stand. (U.S.) Circ. No. 467 (U.S. GPO, Washington, D.C., 1949), Vol. I.

[37]E. J. McGuire, Phys. Rev. A **3**, 1801 (1971).

[38]K. Siegbahn, C. Nordling, G. Johansson, J. Hedman, P. F. Heden, K. Hamrin, U. Gelius, T. Bergmark, L. O. Werme, R. Manne, and Y. Baer, *ESCA Applied to Free Molecules* (North-Holland, Amsterdam, 1969).

[39]W. Mehlhorn, W. Schmitz, and D. Stalherm, Z. Phys. **252**, 399 (1972).

[40]G. Johansson, J. Hedeman, A. Berndtsson, M. Klasson, and R. Nilsson, J. Electron Spectrosc. **5**, 985 (1974).

[41]G. H. Wannier, Phys. Rev. **90**, 817 (1953).

[42]D. Graef, thesis, Wuertsburg, 1986.

[43]G. C. King, M. Tronc, F. H. Read, and R. C. Bradford, J. Phys. B **10**, 2479 (1977).

[44]N. Oda, Radiat. Res. **64**, 80 (1975).

[45]P. van der Straten, R. Morgenstern, and A. Niehaus, Z. Phys. D **8**, 35 (1988).